THE JOURNAL OF PHYSICAL CHEMISTRY B

Article

pubs.acs.org/JPCB

Determination of Chain Flip Rates in Poly(ethylene) Crystallites by Solid-State Low-Field ^{1}H NMR for Two Different Sample Morphologies

R. Bärenwald,[†] Y. Champouret,[‡,§] K. Saalwächter,*[,†] and K. Schäler*[,†]

[†]Institut für Physik − NMR, Martin-Luther-Universität Halle-Wittenberg, Betty-Heimann-Str. 7, D-06120 Halle, Germany

[‡]Department of Materials, Loughborough University, Loughborough, LE11 3TU, U.K.

[§]The Dutch Polymer Institute (DPI), P.O. Box 902, 5600 AX Eindhoven, The Netherlands

ABSTRACT: Using simple and cheap low-field ^{1}H NMR methods such as the magic sandwich echo technique and FID component analysis, we determine jump rates for 180° chain flips in poly(ethylene) (PE) crystallites, which are comparable to literature data obtained from advanced, complex, and time-consuming ^{13}C-based NMR methods. In the investigated temperature range, we find similar jump rates for the local chain flip process in a melt-crystallized sample containing lamellar crystals with disordered fold surface and in reactor powder samples having a rather adjacent-reentry-like structure. Previous NMR studies of Yao et al. revealed different chain diffusion coefficients for the resulting long-range chain diffusion between amorphous and crystalline regions in melt- vs solution-crystallized (adjacent reentry) samples. From our results, we conclude that, in the investigated temperature range, the fold surface, which presumably influences the effective chain transport, does not have a strong effect on the time scale of the local chain flip process. We confirm an Arrhenius temperature dependence of the jump rate for the local flip process and calculate activation energies which show a slight trend toward smaller values for the reactor powders (~76 kJ/mol) in comparison to the melt-crystallized sample (~103 kJ/mol).

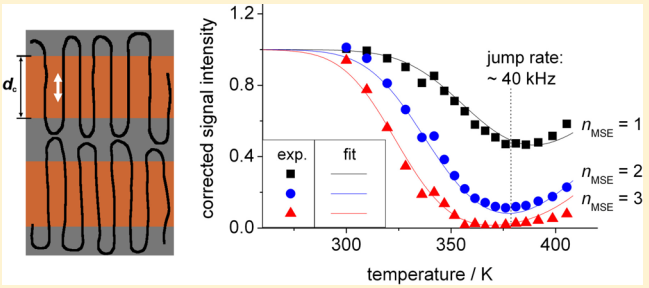

INTRODUCTION

As the chemically simplest polymer, poly(ethylene) (PE) is a standard material with many industrial applications. Therefore, obtaining information about the origin of its special mechanical properties is of great importance. PE is semicrystalline and has been investigated intensively, for example, with regard to crystallinity[1] and chain dynamics.[1−4]

Like isotactic poly(propylene) (iPP), poly(oxymethylene) (POM), or poly(ethylene oxide) (PEO), PE is α_c-mobile;[5] i.e., the chains perform helical jump motions within the crystallites. In the special case of PE, the CH_2-groups flip by 180° around the chain axis. During such a jump, a chain simultaneously translates by one CH_2-group so that it is again in its energetically most favorable position and fits into the lattice perfectly before and after the jump.[4] Repeated flip processes may allow chains to move through the crystallite, i.e., to diffuse over a rather long distance. This feature results, e.g., in the ultradrawability of PE fibrils, because long-range rearrangements of chains in the crystallites facilitate the generation of highly extended crystalline PE chains by drawing.[5] Hence, the chain flip motion influences technologically relevant mechanical properties of the polymer, for instance, drawability[5] and creep,[6] as well as crystallinity[7] and crystal thickening.[7,8]

In their work, Yao et al.[9] show that the diffusion coefficient and thus the speed of long-range chain diffusion depends on the morphology of the PE sample. In their article, they compare diffusion coefficients for chain diffusion between amorphous and crystalline regions of a melt-crystallized and a solution-crystallized sample. Both samples are chemically identical but differ in morphology and chain mobility. While the melt-crystallized sample shows a rather switchboard-like structure and nearly isotropic mobility of chains in the noncrystalline regions, the solution-crystallized sample exhibits an adjacent-reentry-like morphology where noncrystalline regions mainly consist of chain folds, so that chain dynamics here are much more restricted than in the melt-crystallized sample.[3] Yao et al. found that the solution-crystallized sample featured a higher diffusion coefficient than the melt-crystallized sample over the whole temperature range they investigated.[9] At first sight, this appears counterintuitive. One would expect easier and faster chain movements in the crystallites of the melt-crystallized sample with its more flexible chains in the noncrystalline regions. Yao et al. explain their observation by the smaller structural difference between the crystalline and noncrystalline regions in the solution-crystallized sample, which results in a

Received: June 22, 2012
Revised: September 6, 2012
Published: October 22, 2012

smaller entropy difference and thus facilitates the exchange between the regions compared to the melt-crystallized sample.

These findings raise the question whether the macroscopic difference in chain diffusion coefficients in the different sample morphologies is based on a difference in the time-scale of the local 180° chain flip process. We address this topic by applying a solid-state low-field ^{1}H NMR technique.

NMR experiments are sensitive to the mobility of polymer chains and are therefore in principle applicable for the investigation of polymer dynamics in a wide range of correlation times between picoseconds and seconds.[10] Unfortunately, the local chain flip motion in PE crystallites is difficult to investigate by NMR, as, due to the all-trans conformation of the chain, a 180 flip changes the orientation of the C−H and H−H internuclear vectors by 180°, which leaves dipolar couplings, chemical shifts, and ^{2}H quadrupolar interactions almost unchanged. Hence, complex tricks are needed in order to allow the identification of this process at all. An elegant but expensive and time-consuming method was presented by Hu, Boeffel, and Schmidt-Rohr.[2] They made a preparative effort using melt-crystallized high-density (HD) PE labeled with dilute ^{13}C−^{13}C spin pairs. With the aid of dipolar coupling-based stimulated-echo experiments, they proved that 180° chain flips occur indeed, using the fact that the echo intensity decay is a measure of the population of ^{13}C−^{13}C-bond orientations parallel to their initial orientation. In a further approach, they investigated the changes in 1D ^{13}C line shapes at varying temperature for spins in the crystalline regions to gain motional rates of the flip process.

Here, we use a simple low-field ^{1}H NMR method to obtain information about chain flip rates in PE crystallites. We detect the dipolar coupling strength between protons in the crystallites indirectly. In general, the dipolar coupling constant between two protons j and k depends on the distance r_{jk} between them and on the angle Θ_{jk} between the interconnection vector of the two protons and the magnetic field. The total coupling strength can be calculated as a sum of the individual couplings. The strong dipolar coupling between the two protons bonded to one carbon (geminal coupling) is invariant under the 180 chain flip, as r_{jk} and Θ_{jk} do not vary due to the jump motion. However, the weaker secondary longer-range couplings change when chains move. When the motion is fast enough, we measure a coupling constant for averaged proton positions which differs from the coupling strength in a rigid system. We exploit this fact in order to determine the jump rate of the flip process.

For our measurements, we use the magic sandwich echo (MSE) pulse sequence.[11] It refocuses a signal which was lost due to the action of multiple dipolar couplings. Its efficiency depends systematically on the change of dipolar couplings due to molecular dynamics in the sample, so that these dynamics are detectable.

EXPERIMENTAL SECTION

Samples. In this work, we investigated three different PE samples with two different morphologies. Figure 1 shows their structure schematically.

A commercial HD PE sample with a weight-averaged molecular weight M_w ∼ 349 kg/mol and a polydispersity PD ∼ 21.4 (as measured by gel permeation chromatography (GPC)) was provided by Basell Polyolefine GmbH. As it was crystallized from the melt, it exhibits lamellar crystals with disordered fold surfaces (see Figure 1a). Resulting from the high polydispersity the sample contains short chains possibly forming tight folds at crystalline surfaces as well as long chains which can entangle in noncrystalline regions. The crystallinity amounts to 59% (mass crystallinity) or 55.4% (volume crystallinity), determined by differential scanning calorimetry (DSC) and wide-angle X-ray scattering (WAXS), respectively. Results from small-angle X-ray scattering (SAXS) reveal a long period L ∼ 21 nm. The lamellar thickness d_c ∼ 13 nm was estimated using the crystallinity data. The melting temperature was quantified to be 405 K by DSC (heating rate: 20 K/min). For comparison, we further investigated two ultrahigh-molecular-weight (UHMW) PE reactor powder samples. For further information about sample preparation and properties, see ref 12. These samples both show a rather adjacent-reentry-like morphology but differ in molecular weight (M_w ∼ 5000 kg/mol and 750 kg/mol) and polydispersity (PD ∼ 3 and 1.8, respectively), derived from rheology. The lamellar thickness of both samples was estimated to about 7 nm by transmission electron microscopy (TEM). All three samples exhibit the orthorhombic unit cell as is usual for PE under atmospheric pressure.

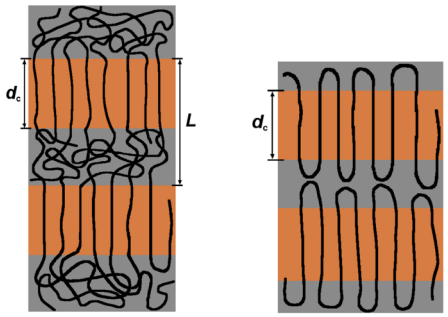

Figure 1. Schematically drawn, idealized morphologies of the investigated samples: (a) melt-crystallized PE, the structure of which resembles a switchboard-model-like morphology with disordered fold surfaces; (b) PE reactor powder showing a rather adjacent-reentry-like structure with tight folds.

As a reference substance, we used poly(ε-caprolactone) (PCL). PCL resembles PE in chain conformation and unit cell geometry of the crystallites. Like the chains of PE, those of PCL contain CH_2 groups crystallizing in a planar all-trans conformation and forming an orthorhombic unit cell with dimensions a = 7.496 Å and b = 4.974 Å perpendicular to the chain axis similar to those of PE (a = 7.42 Å, b = 4.95 Å).[13] The repeat units in PCL are of course significantly longer than in PE due to additional ester groups replacing every sixth CH_2 group. These ester groups are slightly twisted out of the plane formed by the CH_2 groups and cause an elongation of the PCL unit cell in the chain direction (c = 17.297 Å) compared to PE (c = 2.534 Å). Unlike PE, PCL is crystal-fixed;[5,14] i.e., the chains do not translate through the crystallites. The PCL sample with M_w ∼ 63.8 kg/mol and PD ∼ 1.5 was purchased from Sigma Aldrich.

NMR Spectroscopy. The ^{1}H low-field time-domain measurements were carried out on a Bruker minispec mq20 spectrometer with a static magnetic field of 0.5 T and a ^{1}H Larmor frequency of 19.95 MHz equipped with a commercial wide temperature range static probe. The spectrometer features a 90° pulse length of 1.6 μs and a receiver dead time of 15 μs. The samples were packed into 10 mm NMR sample tubes in the form of small pieces. For measurements, each sample was

dx.doi.org/10.1021/jp3061625 | J. Phys. Chem. B 2012, 116, 13089−13097

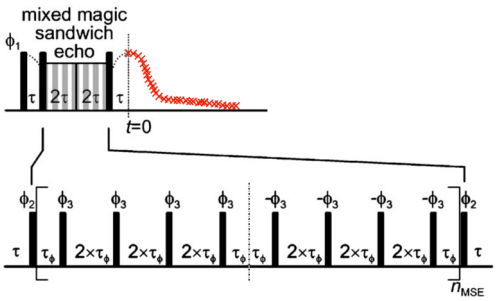

Figure 2. Pulse sequence for the magic sandwich echo (MSE). The waiting time τ depends on the phase-switching time τ_Φ, the 90° pulse length τ_{p90}, and the number of cycles n_{MSE}: $\tau = (2\tau_{p90} + 4\tau_\Phi)n_{MSE}$. The sequence length t_{seq} is calculated as $t_{seq} = 6\tau$. The phase cycle is $\Phi_1 = x\bar{x}\bar{x}x\bar{x}\bar{x}x$, $\Phi_2 = \bar{y}yy\bar{y}\bar{x}x\bar{x}x$, $\Phi_3 = xxxx\bar{y}\bar{y}\bar{y}\bar{y}$.

placed in the center of the magnet. In order to keep the sample completely in the region of highest homogeneity of the magnetic field, we only filled the lowermost 6 mm of the tubes. The sample temperature was regulated by means of a BVT3000 heater. A cooler was needed for temperatures below 300 K. We used air as the heat-transfer medium for heating and cooling. The temperature at the sample position could be set with an uncertainty of about 1 K and a temperature gradient over the sample of 0.5 K. At distinct measurement temperatures in the investigated range (from ∼240 to ∼400 K), the longitudinal relaxation time T_1 was determined via a saturation recovery experiment in order to estimate the recycle delay rd = $5T_1$ for all samples. We used rd = 2−4.8 s and rd = 1.2 s for PE and PCL, respectively. The signal was detected on-resonant and in absorptive mode, analyzing the real part of the complex time-domain signal. The number of scans was varied between 16 and 128 in order to ensure a sufficiently high signal-to-noise ratio.

For investigating chain dynamics in the PE samples, we used the magic sandwich echo (MSE) sequence, as shown in Figure 2. It refocuses the rapidly decaying signal after a 90° pulse which is governed by strong ^{1}H dipole−dipole interactions. The echo produced by the sequence appears after a distinct time after the last pulse. By choosing this waiting time at least as long as the receiver dead time of the apparatus, a virtually dead-time free induction decay (FID) can be acquired, starting on the echo top.

The pulsed MSE sequence we used here contains a 90° pulse followed by a waiting period τ and the actual *sandwich* part consisting of two 90° pulses of the same phase and two blocks of four 90° pulses each in between. All pulses within one block have the same phase, and the phase of the second block is shifted by 180° compared to the one of the first block (see Figure 2). After another waiting time τ, the echo is acquired.[15] Compared to the original MSE sequence, we apply a so-called mixed version which combines the MSE with a Hahn echo for additionally refocusing losses due to inhomogeneities of the magnetic field by using a virtual composite pulse as a last pulse,[16,17] just by inverting its phase.

As described, e.g., in ref 16, the mode of action of the pulse sequence can be understood with the aid of Average Hamiltonian theory. The Hamiltonian of the spin system during radio frequency irradiation can be calculated via transition into a doubly rotating frame. After the first 90° pulse in the MSE sequence, the transverse magnetization develops under the dipolar Hamiltonian $\hat{H}_D$ during the time period τ. In the following *sandwich* part, the magnetization evolves further under $-0.5\ \hat{H}_D$ during a time period of 2τ. Thus, after a time of 3τ, the zeroth-order Average Hamiltonian is zero and the signal is refocused completely. Therefore, an echo already appears in the middle of the pulse sequence which, however, cannot be acquired completely because the time interval τ_Φ between the last pulse and the echo is shorter than the receiver dead time. During the second half of the sequence, the magnetization develops inversely, so that another echo appears at 6τ.[16]

The MSE sequence only refocuses the signal properly if the following two conditions are fulfilled:

(1) The relation $1/(4\tau) \gg \omega^D$ must apply for the waiting time τ in the sequence, with ω^D being the dipolar coupling strength between protons. The length of each of the blocks consisting of four 90° pulses as well as the total time between the two flanking sandwich pulses has to be short compared to the reciprocal dipolar coupling strength. If this condition is not met, higher-order terms of the Average Hamiltonian cannot be neglected anymore, and the Hamiltonian does not reduce to zero at the end of the sequence, resulting in an echo attenuation which is proportional to τ^2.[11,18,19]

(2) During the whole sequence, ω^D needs to stay constant. Otherwise, the dipolar Hamiltonian changes during the sequence and is not reduced to zero at the end.

This last fact can be used to detect chain flip motions on the time scale of the sequence length by using the systematic signal loss caused by the jump motion. Lengthening the sequence increases the probability for jump motions to occur during the sequence. If the correlation time of the motion is on the order of the sequence length, a higher number of jumps during the sequence results in a stronger change of ω^D, leading to less efficient refocusing and thus to signal loss. For investigating chain dynamics in the sample quantitatively, we examine the echo-height dependence on the sequence length for different temperatures.

The MSE pulse sequence can be extended either by lengthening the time interval τ_Φ between two pulses or by increasing the number n_{MSE} of sandwich blocks (see Figure 2). Because the signal loss with increasing sequence length t_{seq} is faster and more complex for the first version,[15] we decided to vary n_{MSE}. To realize smaller sequence length increments, one can reduce the number of 90° pulses in the basic *sandwich* blocks from four to two. Unfortunately, on our machine, the performance for such *half* block lengths is worse than with the original four pulses; i.e., less signal is detected due to unavoidable problems related to radio frequency pulse quality.

Data Analysis. For various temperatures below the melting point of the samples, the free induction decay (FID) detected after a simple 90° pulse and after MSEs of different sequence lengths were acquired. Note that the term "FID signal" henceforth just relates to signals detected without MSE, and FIDs with MSE are called "MSE signal". Variation of the sequence length was accomplished by increasing the number n_{MSE}, accordingly prolonging the times τ flanking the *sandwich* part. The measurement of a full set of data at one measurement temperature with 128 scans and rd = 2 s took about 1 h.

In order to enable a FID signal normalization, which is necessary for the shape parameter determination (see below), for each sample, we additionally measured a FID at a temperature T_{am} above the melting point after all other experiments had been completed. For the fully amorphous,

dx.doi.org/10.1021/jp3061625 | J. Phys. Chem. B 2012, 116, 13089−13097

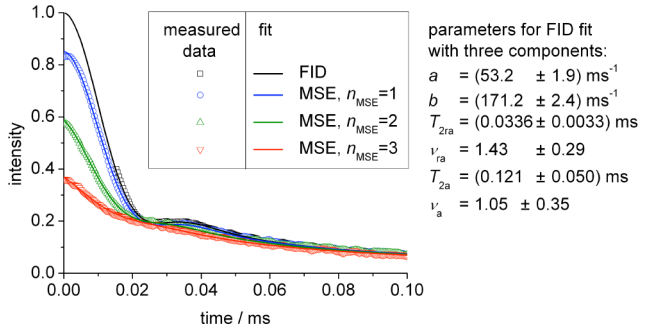

Figure 3. FID and MSE curves of the melt-crystallized PE sample at $T \approx 330$ K for different sequence lengths, each fitted with a three-component function according to eq 2.

molten sample at T_{am}, the initial intensity $I_{am}(t = 0)$ is easily assessed via extrapolation. The signal intensity $I(t,T)$ of FIDs and MSEs at different temperatures T was then made comparable by normalization and temperature correction according to Curie's law: $I_{norm}(t,T) = (I(t,T) \times T)/(I_{am}(t = 0) \times T_{am})$.

The FID and MSE signals (see Figure 3) each contain contributions from rigid and mobile sample components. Signal decomposition can be done by using appropriate fit functions for the different sample fractions.[20] As chain dynamics in crystalline regions are strongly anisotropic, they hardly average proton dipolar couplings. The resulting strong dipolar interactions cause a fast dephasing of precessing nuclear dipoles and induce a fast signal decay at short acquisition times. This rapid decay can be described by an Abragam function, $\exp(-0.5(at)^2)\cdot\sin(bt)/(bt)$, which is similar to a series (moment) expansion of the FID for strongly coupled spins.[21] From the parameters a and b of the Abragam function, the second moment of line shape M_2 can be calculated:

$$M_2 = a^2 + \frac{1}{3}b^2 \tag{1}$$

It is a measure of the line width in the spectral (frequency) domain, and therefore of the strength of the dipolar couplings. We note that time-domain fitting provides more accurate data for the second moment than integration of spectra, the latter being subject to baseline problems. Although dipolar couplings are strong between protons in the crystallites in principle, the anisotropic chain motion nevertheless results in partial averaging of couplings if the motional rate exceeds the dipolar coupling strength (~20 kHz). Thus, molecular motions may lead to a reduced line width and M_2 compared to the static case, turning M_2 into an indicator for chain motions in crystallites (see Results).[1,22]

The slow long-time signal decay in FID and MSE is caused by protons in the amorphous regions, where dipolar interactions are averaged to a high extent due to fast chain motions which are much more isotropic than in the crystallites. The averaging results in a slower dephasing of the precessing nuclear dipoles after the 90° pulse. As long as the fit interval is suitably restricted (to account for the incomplete knowledge on the functional form of the total decay), the amorphous phase signal can conveniently be described by a modified (stretched or compressed) exponential function: $\exp(-(t/T_{2a}^*)^{\nu_a})$.[15]

Many authors furthermore state the existence of a rigid-amorphous interphase in PE, see e.g., refs 23−29. In our investigations, we also find such a phase of intermediate mobility, the signal of which we once again describe by a modified exponential function: $\exp(-(t/T_{2ra}^*)^{\nu_{ra}})$. A satisfactory fitting quality could only be realized using three components; hence, the first 200 μs of the FIDs were fitted with the following function:

$$I_{norm}^{Fit}(t) = f_c e^{-0.5(at)^2} \frac{\sin bt}{bt} + f_{ra} e^{-(t/T_{2ra}^*)^{\nu_{ra}}} + f_a e^{-(t/T_{2a}^*)^{\nu_a}} \tag{2}$$

At longer acquisition times, the signal is strongly influenced by the inhomogeneity of the magnetic field and does not reveal additional valuable information on the dynamics or structure of the sample. Signal decomposition using this fit function can only be achieved for data measured at a temperature far above the glass transition temperature of the bulk amorphous phase, at which strong mobility differences of the chains in the different phases are present.

The additional normalization condition $f_c + f_{ra} + f_a = 1$ was added to ensure stability of the fit to the FID. All shape parameters (a, b, T_{2ra}^*, T_{2a}^*, ν_{ra}, ν_a) were free parameters in the fits, and showed a continuous and smooth temperature dependence, confirming their plausibility. For fitting the data for the MSE curves, we used the shape parameters resulting from the fit to the FIDs detected at the same temperature as fixed parameters, leaving only the signal fractions f_c, f_{ra}, and f_a as free parameters.

The signal echos did not exactly appear at the expected position in time but at a shifted position depending on the sequence length t_{seq}, which is most probably due to technical imperfections. Although this shift is rather small (0.1−6 μs), it affects the fitting in a non-negligible way. We therefore introduced an additional fit parameter Δt into expression 2 for the MSE fits, replacing t by $t + \Delta t$. As it is difficult to estimate the shift Δt for the faint echos after long sequence lengths t_{seq}, moreover, we determined Δt as a function of t_{seq} for short sequence lengths (n_{MSE} = 1, 2, 3) and did a linear extrapolation to obtain Δt for long sequence lengths (n_{MSE} = 4, 5, 6), where we fixed Δt in the MSE fits.

RESULTS

Crystallinity. The mass fractions of the crystalline, rigid-amorphous, and amorphous sample components are represented by the signal fractions (f_c, f_{ra}, and f_a) in the FID fit function. Figure 4 exemplarily shows the temperature dependence of these fractions for two of our samples. From the scatter of the data points, we estimate the relative uncertainty to be 5% of each particular fraction f_c, f_{ra}, and f_a. It is mainly attributed to fitting stability. The glass transition temperature T_g of about 150 K for PE[30] is well below the measured temperature range. Around 400 K, the crystalline fraction decreases rapidly and accordingly the amorphous fraction increases with rising temperature for both samples. The melting temperature T_{melt} ~ 405 K from DSC measurements for the melt-crystallized sample matches well the melting temperature range shown in Figure 4.

Morphological differences of the samples are confirmed by the sample fractions determined herein. The mobile-amorphous fraction of the reactor powder sample is close to zero because, in our approach, the tight chain folds at crystallite surfaces are not counted as mobile-amorphous but as rigid-amorphous fraction due to their low mobility. Contrary to the reactor powder, the melt-crystallized sample shows a clearly detectable mobile-amorphous fraction and a lower crystallinity

dx.doi.org/10.1021/jp3061625 | J. Phys. Chem. B 2012, 116, 13089−13097

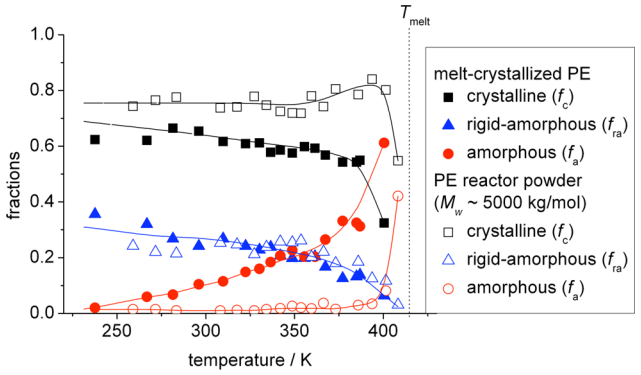

Figure 4. Temperature dependence of crystalline, rigid-amorphous, and amorphous mass fractions (f_c, f_{ra}, and f_a) in the melt-crystallized PE and in a reactor powder sample (M_w ~ 5000 kg/mol) obtained from FID fitting. The continuous lines serve as guides to the eye. The melting temperature T_{melt} is represented by the dashed line.

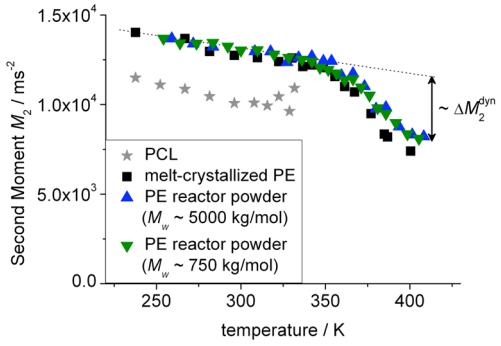

Figure 5. Temperature dependence of the second moment M_2 of the line shape calculated from FID fit parameters according to eq 1. ΔM_2^{dyn} denotes the decay of the second moment due to chain dynamics (see text).

of ~60% at ambient temperature (see Figure 4), which matches well the DSC value of 59%. Both samples show a rather high amount of rigid-amorphous phase, the quantification of which strongly depends on the fit function chosen by us.

Chain Dynamics in the Crystallites. *Dipolar Second Moment of the Line Shape in Crystallites.* As already mentioned in the description of the data analysis, the second moment M_2 of line shape can be calculated for the crystalline sample fraction from the FID fit parameters according to eq 1. Figure 5 shows the resulting M_2 values and their temperature dependence. The decrease of M_2 with rising temperature for the melt-crystallized PE sample and the two reactor powders fits literature data for a melt-crystallized sample investigated by Olf and Peterlin[1] rather well. The slight decay at temperatures below 360 K is caused by lattice expansion due to oscillations about the chain axis on a time scale of picoseconds.[31,32] At higher temperatures, this decay accelerates due to chain dynamics in the crystallites. However, PCL only exhibits a slight decrease caused by lattice expansion. A second, faster decay is missing here, confirming the lack of large-amplitude chain mobility in PCL crystallites.

Jump Rate Determination by Means of the MSE Pulse Sequence. By fitting expression 2 to the MSEs, we determined the signal fraction f_c of the crystalline phase depending on the sequence length t_{seq}. The FID is considered as MSE with t_{seq} = 0, and therefore, the data curves $I_c(t_{seq}) = f_c(t_{seq})/f_c(0)$ were normalized to the crystalline fraction $f_c(0)$ determined from the corresponding FID, (see Figure 6). The signal fraction of the crystalline phase decreases with increasing sequence length because the conditions for optimum signal refocusing mentioned in the Experimental Section are not fulfilled. Beside chain dynamics, also too strong dipolar interactions lower the refocusing efficiency. This can be concluded from the fact that $I_c(t_{seq})$ also decays for PCL where no chain dynamics is present in the crystallites, and for all PE samples at low temperatures where chain dynamics is too slow for a jump process to be probable during the sequence duration. However, in order to determine a jump rate quantitatively, we had to isolate the decay $I_c^{corr}(t_{seq})$ which is arising from intermediate-regime chain dynamics only.

For this reason, we fitted modified exponential functions to the curves $I_c(t_{seq})$ (see Figure 6a):

$$I_c^{fit}(t_{seq}) = e^{-(t_{seq}/T_2^*)^\beta} \quad (3)$$

The temperature dependence of the resulting parameters T_2^* and β is shown in Figure 7.

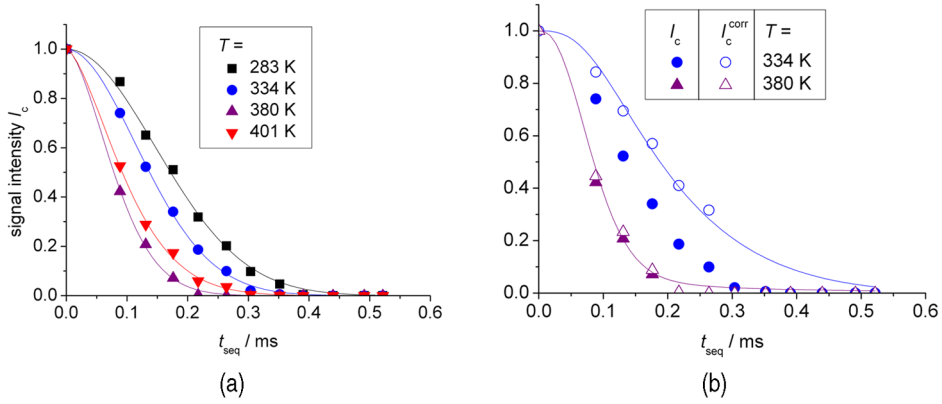

Figure 6. Intensity of the crystalline-phase signal depending on the length of the MSE sequence for different temperatures for a PE reactor powder sample (M_w ~ 5000 kg/mol). In part a, the signal intensity is normalized to the crystalline fraction determined from the FID, and in part b, it is additionally corrected with regard to the deleterious action of strong static dipolar interactions on the MSE performance according to eq 4. The measured data are represented by symbols. The continuous lines are fits according to the empirical function eq 3 in (a) and to eq 7 for jump rate determination in (b), respectively.

dx.doi.org/10.1021/jp3061625 | J. Phys. Chem. B 2012, 116, 13089−13097

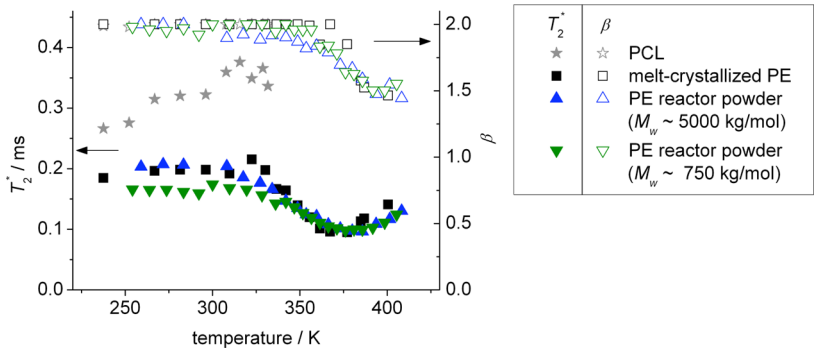

Figure 7. Temperature dependence of the fit parameters T_2^* and β determined from fits to $I_c(t_{seq})$ by eq 3 for different PE samples and the PCL reference sample.

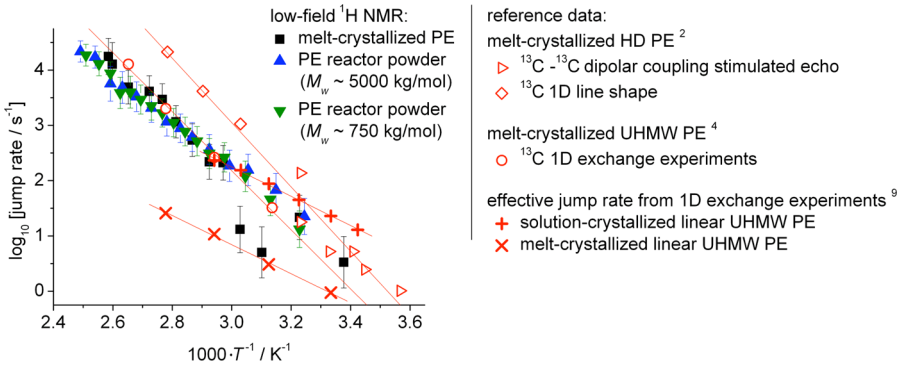

Figure 8. Arrhenius plot of the jump rates for the different PE samples in comparison with literature data.

At low temperatures, we find a Gaussian curve shape ($\beta \approx 2$) which indicates a decay dominated by imperfection terms related to strong static dipolar couplings (as described in the section "NMR Spectroscopy"). At high temperatures, the curve shape is influenced by chain dynamics, resulting in $\beta < 2$.

The characteristic decay time T_2^* shows a minimum when chain dynamics occur on the time scale of the sequence length. Note that T_2^* is not a *real* T_2 relaxation time because it does not only contain information about dynamics but is also influenced by strong static dipolar interactions and by additional refocusing problems caused by our minispec device.

We corrected $I_c(t_{seq})$ with regard to strong static dipolar interactions by multiplication with a Gaussian function:

$$I_c^{corr}(t_{seq}) = I_c(t_{seq}) \cdot e^{(t_{seq}/T_2^{*corr})^2} \quad (4)$$

where

$$T_2^{*corr}(M_2) = A + BM_2$$

Here we exploited the linear correlation between M_2 and T_2^* which results from the dependency of M_2 and T_2^* on the dipolar coupling strength and arises for PCL and PE at low temperatures, i.e., in the absence of large-amplitude chain dynamics. The parameters A and B were determined by a linear fit. Additionally, the parameter A was refitted for each sample separately, so as to provide the best possible equivalence of the calculated T_2^{*corr} and the value T_2^* measured at low temperatures.

A Gaussian correction function was chosen because it describes the influence of static dipolar couplings (see Figure 7 and text above). As a result, the corrected decays $I_c^{corr}(t_{seq})$ only depend on chain dynamics, so that $I_c^{corr}(t_{seq}) \approx 1$ applies for PCL and PE at low temperatures.

In the following section, the data sets $I_c^{corr}(t_{seq})$ are analyzed quantitatively to determine the correlation time τ_c and the jump rate $1/(2\tau_c)$. By means of the Anderson–Weiss theory,[33] Fechete and co-workers derived a fit function for the initial part of $I_c^{corr}(t_{seq})$.[17] In their work, they applied a single exponential correlation function to describe motions on a time scale of μs. For fitting the whole decay, we extended Fechete's function to a larger range of t_{seq} by considering also higher even moments of line shape and ascribing them to the second moment M_2. The resulting function

$$S_{MSE}(t_{seq}, \Delta M_2^{dyn}, \tau_c) = \exp\left[-\Delta M_2^{dyn}\tau_c^2\left(e^{-t_{seq}/\tau_c} - 3e^{-5t_{seq}/6\tau_c} + \frac{9}{4}e^{-2t_{seq}/3\tau_c} + 3e^{-t_{seq}/6\tau_c} + \frac{t_{seq}}{2\tau_c} - \frac{13}{4}\right)\right] \quad (5)$$

depends on the correlation time τ_c of the jump motion and on the decay ΔM_2^{dyn} of M_2 due to the flip process. From Figure 5, we estimate $\Delta M_2^{dyn} \approx 4000$ kHz^2. However, the fits of $S_{MSE}(t_{seq},\Delta M_2^{dyn},\tau_c)$ to our data curves $I_c^{corr}(t_{seq})$ do not match well. Presumably, this is due to a distribution of correlation times τ_c of the jump motion as opposed to a single τ_c value, as already demonstrated by Hu et al., who found that the correlation function for chain flips in PE crystallites is better described by a stretched exponential than by a single exponential function.[2] For this reason, we additionally assumed a log-normal distribution of the correlation time

$$p(\tau_c, \mu, \sigma) = \frac{1}{\sqrt{2\pi}\sigma\tau_c} e^{-(\ln \tau_c - \mu)^2/2\sigma^2} \quad (6)$$

dx.doi.org/10.1021/jp3061625 | J. Phys. Chem. B 2012, 116, 13089–13097

containing the parameters μ and σ, the latter being an approximation for the width of the distribution in decades. We fitted the final function

$$S_{MSE}^{distr}(t_{seq}, \Delta M_2^{dyn}, \mu, \sigma) = \int_0^\infty p(\tau_c, \mu, \sigma) S_{MSE}(t_{seq}, \Delta M_2^{dyn}, \tau_c)\, d\tau_c \quad (7)$$

to our data curves $I_c^{corr}(t_{seq})$ using fixed parameters ΔM_2^{dyn} and σ (see below for the values chosen), while μ was left as a free parameter to be determined by fitting. The integration was done numerically using the program OriginPro 7.5. As can be seen in Figure 6b, $S_{MSE}^{distr}(t_{seq},\Delta M_2^{dyn},\mu,\sigma)$ yields good fits to our data. We define the mean

$$\langle \tau_c \rangle = \exp(\mu + \sigma^2/2) \quad (8)$$

of the τ_c distribution as an appropriate result to describe the correlation times in the samples. Accordingly, the jump rate is given by $1/(2\langle\tau_c\rangle)$. Furthermore, we chose the parameter values of σ and ΔM_2^{dyn} in a way that in an Arrhenius plot the resulting temperature dependence of the jump rate does not show any discontinuity or sharp bend. In so doing, we found a straight line in the Arrhenius plot (see Figure 8). For the estimation of uncertainties, σ and ΔM_2^{dyn} were chosen as large as and as small as possible so that a straight line persists in the Arrhenius plot. Because the data quality of $I_c^{corr}(t_{seq})$ was better for the reactor powder sample with $M_w \sim 750$ kg/mol than for the other two, we determined σ and ΔM_2^{dyn} for this sample as described above and used the same values for the other samples.

Figure 8 shows the resulting data points. Two important facts can be concluded from the plot. First, all samples show nearly the same temperature trend of the jump rate $1/(2\langle\tau_c\rangle)$ in the investigated temperature range. Slight deviations might occur due to different data quality. Second, we can state an Arrhenius dependence of the correlation time $\langle\tau_c\rangle$ on the temperature T:

$$\langle \tau_c \rangle = \tau_c^0 e^{E_a/(RT)} \quad (9)$$

Results for the activation energy E_a and the prefactor τ_c^0 obtained from linear fits to the data in Figure 8 are reported in the upper part of Table 1. We estimated the uncertainties of E_a and $\log_{10}[\tau_c^0]$ by determining their maximum and minimum values using the range of possible jump rates given by the error bars in Figure 8.

Table 1. Comparison of Results from Different Methods of Data Analysis

	melt-cryst. PE	PE reactor powder, $M_w \sim$ 750 kg/mol	PE reactor powder, $M_w \sim$ 5000 kg/mol
Analysis of $I_c(t_{seq})\|_{T=const}$			
ΔM_2^{dyn} (kHz^2)	6700 ± 800	6700 ± 800	6700 ± 800
σ (kHz^2)	1.57 ± 0.23	1.57 ± 0.23	1.57 ± 0.23
E_a (kJ·mol^{-1})	97 ± 45	80 ± 17	72 ± 19
$\log_{10}[\tau_c^0(s)]$	−17.6 ± 6.4	−15.0 ± 2.3	−14.0 ± 2.8
Analysis of $I_c(T)\|_{t_{seq}=const}$			
ΔM_2^{dyn} (kHz^2)	5200	5910 ± 370	7820 ± 550
σ (kHz^2)	0.94	1.41 ± 0.12	2.02 ± 0.15
E_a (kJ·mol^{-1})	109.2 ± 4.2	77.3 ± 2.3	74.5 ± 2.5
$\log_{10}[\tau_c^0(s)]$	−19.86 ± 0.61	−14.81 ± 0.29	−13.70 ± 0.33

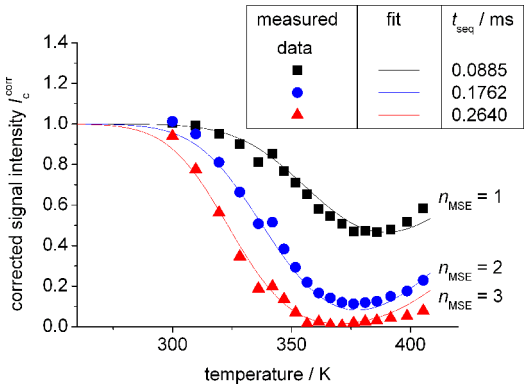

Figure 9. Crystalline-phase signal intensity (normalized and corrected with regard to strong dipolar interactions according to eq 4) depending on temperature for three different MSE sequence lengths for a PE reactor powder sample ($M_w \sim 750$ kg/mol). Data points and fits with $S_{MSE}^{distr}(T,t_{seq},\Delta M_2^{dyn},E_a,\tau_c^0,\sigma)$ are shown.

In the approach described before, we fitted $I_c^{corr}(t_{seq})$ by $S_{MSE}^{distr}(t_{seq},\Delta M_2^{dyn},\mu,\sigma)$ with fixed parameters ΔM_2^{dyn} and σ, and determined μ for every temperature. We refer to this method as the analysis of $I_c(t_{seq})|_{T=const}$. However, data analysis can be simplified and accelerated knowing now that $\langle\tau_c\rangle$ indeed follows an Arrhenius dependence. For fitting the data for all temperatures in one go we derived

$$\mu = \ln \tau_c^0 + \frac{E_a}{RT} - \frac{\sigma^2}{2}$$

from eqs 8 and 9. By help of this relation, we replaced the parameter μ in S_{MSE}^{distr} by T, E_a, and τ_c^0 obtaining a fit function $S_{MSE}^{distr}(T,t_{seq},\Delta M_2^{dyn},E_a,\tau_c^0,\sigma)$ which depends on the temperature T.[34] Data curves $I_c^{corr}(T)$ for fixed t_{seq} could be fitted with this function $S_{MSE}^{distr}(T,t_{seq},\Delta M_2^{dyn},E_a,\tau_c^0,\sigma)$ now. The sequence length t_{seq} enters the fit as a fixed parameter. Therefore, we refer to this method as the analysis of $I_c(T)|_{t_{seq}=const}$. For raising the fit stability, we fitted the data for n_{MSE} = 1, 2, and 3 simultaneously, gaining a single result for the free fit parameters ΔM_2^{dyn}, σ, E_a, and τ_c^0 for each sample (see Figure 9). For the melt-crystallized sample, we chose ΔM_2^{dyn} and σ in a way that the uncertainty of E_a and τ_c^0 was minimal. Due to the limited data quality, in this case, we had to fix the parameters ΔM_2^{dyn} and σ in order to stabilize the fit. The fitting results and parameter uncertainties as determined by the fit are given in the lower part of Table 1.

As can be seen in Table 1 from the difference of the parameter values for ΔM_2^{dyn} and σ, we cannot determine them accurately with the two methods of analysis. However, we obtained similar values for E_a and $\log_{10}[\tau_c^0]$ which seemingly do not depend strongly on ΔM_2^{dyn} and σ. We conclude that it is possible to determine the temperature dependence of the jump rate despite uncertain values of ΔM_2^{dyn} and σ.

Both reactor powder samples show almost the same prefactor τ_c^0 and activation energy of $E_a \sim 76$ kJ/mol. The results for the melt-crystallized sample are influenced by limited data quality, as can be seen in the scatter of the data points in Figure 8. Still the value $E_a \sim 103$ kJ/mol determined herein matches well the activation energy of $E_a \sim 100$ kJ/mol from earlier investigations reported in the literature.[2,4] From the diffusion coefficients determined for chain diffusion between crystalline and amorphous regions, Yao et al. calculated an *effective* jump rate for the local flip process serving as a measure

dx.doi.org/10.1021/jp3061625 | J. Phys. Chem. B 2012, 116, 13089−13097

for those chain flips that effectively provide longer-range translational motion of chains. However, measurements of such effective jump rates by Yao et al. for a melt-crystallized and a solution-crystallized sample yield an activation energy of $E_a \sim 50$ kJ/mol,[9] which is smaller than all the values determined by us for the local flip process directly.

In Figure 8, we compare effective and local jump rates from the literature and from our measurements. For this purpose, we have calculated effective jump rates from diffusion coefficients for the solution-crystallized sample investigated by Yao et al., following their considerations given for the melt-crystallized sample in ref 9. As the results are obtained by means of different NMR methods for different samples, we can only compare them qualitatively. All in all, our results match the literature values for local jump rates. As we obtained similar results for the melt-crystallized sample with its disordered fold surfaces and the reactor powders showing an adjacent-reentry-like structure, we conclude that the jump rate for the local 180° chain flip process does not depend strongly on sample morphology, lamellar thickness, or molecular weight in the ranges and for the temperatures investigated herein. However, Yao et al. showed that effective jump rates responsible for long-range chain diffusion do depend on sample morphology.[9] The solution-crystallized sample they investigated shows an effective jump rate which is similar to the local one of all samples compared in Figure 8. However, the effective jump rate of the melt-crystallized sample studied by Yao et al. is smaller than all local jump rates depicted. This finding confirms the assumption of Yao et al. that not every local chain flip in PE crystallites contributes to a translation of the whole polymer chain; i.e., there must be ineffective jumps.[9] Because of a higher number of motional constraints in the amorphous regions of the melt-crystallized sample in comparison to the solution-crystallized one, the chain translation seems to be less effective in the former, i.e., despite of equal local jump rates the diffusion coefficient and therefore the effective jump rate is smaller.

CONCLUSIONS

180° chain flips in PE crystallites are difficult to detect by NMR, as they do not change C−H and H−H dipolar couplings, ^{2}H quadrupolar interactions, and chemical shifts. Hence, only a few quantitative literature data on jump rates exist. Applying simple and cheap low-field ^{1}H NMR methods, we could determine jump rates for the local chain flip process in PE. For this purpose, we used FID component analysis and the MSE pulse sequence, for which the efficiency of the dipolar refocusing depends systematically on dynamics in the sample. Our jump rate results are comparable to values obtained from advanced, complex, and time-consuming ^{13}C-based NMR methods.

With our method, we confirmed the Arrhenius temperature dependence of the mean correlation time of the jump process. This result enabled us to investigate the corresponding activation energy for three PE samples of different morphologies and molecular weights by linear fit in an Arrhenius plot. An additional, easier and faster way to determine an activation energy was found by implementing the Arrhenius dependence directly into the fit of our data.

Interpreting our results, we can state that neither changes in molecular weight (in the range shown here) nor differences in morphology (i.e., disordered fold surfaces as compared to tight folds in an adjacent-reentry-like morphology, as well as differences in domain sizes) exert a large influence on the local jump rate in the temperature window accessible for our measurement. However, the jump rates in the reactor powders show slightly lower activation energies compared to the one of melt-crystallized sample. The present results confirm the differences between local dynamics in PE crystallites and longer-range chain transport, which were pointed out in previous NMR measurements.[9] Further work along these lines, comparing different reactor powders and similar adjacent-reentry samples with their direct melt-crystallized analogues, is in progress.

AUTHOR INFORMATION

Corresponding Author

*E-mail: kay.saalwaechter@physik.uni-halle.de; kerstin.schaeler@physik.uni-halle.de.

Notes

The authors declare no competing financial interest.

ACKNOWLEDGMENTS

Financial support of this work was provided by the DFG (SFB-TRR 102, project A1). We acknowledge S. Rastogi for providing the reactor powder samples and for helpful discussions, A. Seidlitz for performing the SAXS, and S. Goerlitz and the research group *Allgemeine Werkstoffwissenschaften* of Martin-Luther-University Halle-Wittenberg for the TEM measurements. For the melt-crystallized HD PE samples and information about their properties, we thank A. Maus (Basell Polyolefine GmbH). Infrastructural support from the European Union (ERDF programme) is gratefully acknowledged.

REFERENCES

(1) Olf, H. G.; Peterlin, A. *Kolloid Z. Z. Polym.* **1967**, *215*, 97−111.
(2) Hu, W. G.; Boeffel, C.; Schmidt-Rohr, K. *Macromolecules* **1999**, *32*, 1611−1619.
(3) Yao, Y. F.; Graf, R.; Spiess, H. W.; Rastogi, S. *Macromolecules* **2008**, *41*, 2514−2519.
(4) Schmidt-Rohr, K.; Spiess, H. W. *Macromolecules* **1991**, *24*, 5288−5293.
(5) Hu, W. G.; Schmidt-Rohr, K. *Acta Polym.* **1999**, *50*, 271−285.
(6) Ward, I. M.; Wilding, M. A. *J. Polym. Sci., Part B: Polym. Phys.* **1984**, *22*, 561−575.
(7) Boyd, R. H. *Polymer* **1985**, *26*, 323−347.
(8) Seidlitz, A. M.Sc. thesis, MLU Halle-Wittenberg, 2011.
(9) Yao, Y.-F.; Graf, R.; Spiess, H. W.; Lippits, D. R.; Rastogi, S. *Phys. Rev. E* **2007**, *76*, 060801(R).
(10) Levitt, M. H. *Spin Dynamics*; Wiley: London, 2001.
(11) Rhim, W.-K.; Pines, A.; Waugh, J. S. *Phys. Rev. B* **1971**, *3*, 684−696.
(12) Pandey, A.; Champouret, Y.; Rastogi, S. *Macromolecules* **2011**, *44*, 4952−4960.
(13) Bittiger, H.; Marchessault, R. H.; Niegisch, W. D. *Acta Crystallogr., Sect. B* **1970**, *26*, 1923−1927.
(14) Kaji, H.; Horii, F. *Macromolecules* **1997**, *30*, 5791−5798.
(15) Maus, A.; Hertlein, C.; Saalwächter, K. *Macromol. Chem. Phys.* **2006**, *207*, 1150−1158.
(16) Matsui, S. *Chem. Phys. Lett.* **1991**, *179*, 187−190.
(17) Fechete, R.; Demco, D. E.; Blümich, B. *J. Chem. Phys.* **2003**, *118*, 2411−2421.
(18) Demco, D. E.; Johansson, A.; Tegenfeldt, J. *Solid State Nucl. Magn. Reson.* **1995**, *4*, 13−38.
(19) Egger, N.; Schmidt-Rohr, K.; Blümich, B.; Domke, W. D.; Stapp, B. *J. Appl. Polym. Sci.* **1992**, *44*, 289−295.
(20) Hansen, E. W.; Kristiansen, P. E.; Pedersen, B. *J. Phys. Chem. B* **1998**, *102*, 5444−5450.

(21) Derbyshire, W.; van den Bosch, M.; van Dusschoten, D.; MacNaughtan, W.; Farhat, I. A.; Hemminga, M. A.; Mitchell, J. R. *J. Magn. Reson.* **2004**, *168*, 278−283.
(22) Olf, H. G.; Peterlin, A. *J. Polym. Sci., Part A-2: Polym. Phys.* **1970**, *8*, 771−789.
(23) Mandelkern, L. *J. Phys. Chem.* **1971**, *75*, 3909−3902.
(24) Bergmann, K. *J. Polym. Sci., Part B: Polym. Phys.* **1978**, *16*, 1661−1634.
(25) Kitamaru, R.; Horii, F.; Murayama, K. *Macromolecules* **1986**, *19*, 636−643.
(26) Mandelkern, L.; Alamo, R. G.; Kennedy, M. *Macromolecules* **1990**, *23*, 4721−4723.
(27) Cheng, J.; Fone, M.; Reddy, V. N.; Schwartz, K. B.; Fisher, H. P.; Wunderlich, B. *J. Polym. Sci., Part B: Polym. Phys.* **1994**, *32*, 2683−2693.
(28) Lili, Z.; Chen, Q.; Hansen, E. W. *Macromol. Chem. Phys.* **2005**, *206*, 246−257.
(29) Hedesiu, C.; Demco, D. E.; Kleppinger, R.; Buda, A. A.; Blümich, B.; Remerie, K.; Litvinov, V. M. *Polymer* **2007**, *48*, 763−777.
(30) Röthemeyer, F.; Sommer, F. *Kautschuktechnologie*, 2nd ed.; Carl Hanser Verlag: München Wien, 2006.
(31) Strobl, G. R.; Trzebiatowski, T.; Ewen, B. *Prog. Colloid Polym. Sci.* **1978**, *64*, 219−225.
(32) Hentschel, D.; Sillescu, H.; Spiess, H. W. *Makromol. Chem.* **1979**, *180*, 241−249.
(33) Kimmich, R. *NMR Tomography, Diffusometry, Relaxometry*; Springer: Berlin, 1997.
(34) Sturniolo, S.; Saalwächter, K. *Chem. Phys. Lett.* **2011**, *516*, 106−110.